Effect of a current blocking barrier on a 2–6 μm p-GaAs/AlGaAs heterojunction infrared detector

D. Chauhan,[1] A. G. U. Perera,[1,a)] L. H. Li,[2] L. Chen,[2] and E. H. Linfield[2]

[1]*Center for Nano-Optics (CeNO), Department of Physics and Astronomy, Georgia State University, Atlanta, Georgia 30303, USA*
[2]*School of Electronic and Electrical Engineering, University of Leeds, Leeds LS2 9JT, United Kingdom*

We report the performance of a 30 period p-GaAs/Al_xGa_{1-x}As heterojunction photovoltaic infrared detector, with graded barriers, operating in the 2–6 μm wavelength range. Implementation of a current blocking barrier increases the specific detectivity (D^*) under dark conditions by two orders of magnitude to $\sim 1.9 \times 10^{11}$ Jones at 2.7 μm, at 77 K. Furthermore, at zero bias, the resistance-area product (R_0A) attains a value of $\sim 7.2 \times 10^8$ Ω cm^2, a five orders enhancement due to the current blocking barrier, with the responsivity reduced by only a factor of ~ 1.5. *Published by AIP Publishing.*
[http://dx.doi.org/10.1063/1.4952431]

Infrared (IR) detectors and imaging systems are becoming increasingly important in a diverse range of military and civilian applications. In recent years, significant attention has been paid to incorporating current blocking architectures into detector designs. For example, AlGaAs current blocking layers have been utilized in quantum dot IR photodetectors (QDIPs) both to enhance performance[1–6] and to achieve elevated operating temperatures.[7–9] Similarly, in type II InAs/GaSb superlattice (T2SL) IR photodetectors, majority carrier (hole) blocking layers have been implemented,[10] as well as electron blocking and hole blocking unipolar barriers in complementary barrier infrared detectors (CBIRD)[11] and p-type-intrinsic-n-type (PbIbN) photodiodes.[12] Furthermore, dark current suppressing structures were also demonstrated, such as conduction band barriers in nBn photodetectors[13,14] and XBn barrier photodetectors.[15] In general, the main goal in these architectures is to lower the dark current, but with a relatively small compromise to the photocurrent, thus achieving a significant improvement in the specific detectivity (D^*).

Due to the mature growth and established processing technology of p-GaAs/Al_xGa_{1-x}As, these materials systems have become increasingly attractive for demonstrating heterojunction interfacial workfunction IR photodetectors (HEIWIP),[16] which operate up to room temperature.[17] Furthermore, replacing the constant Al_xGa_{1-x}As barrier with a graded barrier, achieved by tuning the Al mole fraction (x), was found to enable photovoltaic operation as well.[18] This is advantageous over photoconductive operation as it offers thermal noise limited performance and reduced power consumption. In this letter, we report the effect of a current blocking barrier (CBB) on a 30 period p-GaAs/Al_xGa_{1-x}As IR detector with graded barriers, which shows a photoresponse at 77 K in the $\sim$2–6 μm range under photovoltaic operation. We observe an approximately five orders of magnitude higher resistance-area product (R_0A) at zero bias, resulting in a two orders of magnitude improvement in D^*, with the responsivity compromised only

by a factor of ~ 1.5 at zero bias, compared to performance without the CBB.

A p-GaAs/Al_xGa_{1-x}As heterojunction IR detector was grown on a semi-insulating GaAs substrate by molecular beam epitaxy[19] (Fig. 1(a)). The active region of the photodetector consists of 30 periods of a 20 nm p-GaAs emitter and 60 nm graded Al_xGa_{1-x}As barrier layer, sandwiched between highly doped p$^+$-GaAs contact layers. The p-GaAs emitters are doped at 1.0×10^{19} cm^{-3} throughout, whereas all Al_xGa_{1-x}As barriers are undoped. A 60 nm graded Al_xGa_{1-x}As CBB layer, followed by another p$^+$-GaAs contact layer, was then grown on top of the active region. As a result, there are three p$^+$-GaAs contact layers—the top (T), middle (M), and bottom (B) contacts, with thicknesses of 0.2 μm, 0.5 μm, and 0.7 μm, respectively. Measurements across the top and bottom (T-B) contacts include the CBB, whilst the middle and bottom (M-B) contacts measure the same mesa without the CBB. Therefore, exactly the same mesa can be studied with the CBB, and without it. The mesas were processed by a combination of conventional photolithography and wet etching, and were followed by Ti/Pt/Au metal evaporation to form metallic contacts on the top, middle, and bottom contact layers. The top and middle (T-M) mesa contacts have areas of 400 μm × 400 μm and 570 μm × 570 μm, respectively. The top p$^+$-GaAs contact layer was partially etched leaving a $\sim$20 nm region, to open an optical window (260 μm × 260 μm, Inset, Fig. 2) for normal incidence, optical illumination.

The valence band offset between the p-GaAs emitter and the undoped Al_xGa_{1-x}As barrier forms a heterojunction, which leads to an interfacial work function,[16] controlled by the mole fraction, x, in the Al_xGa_{1-x}As barrier. The energy difference between the Fermi level and the top of the barrier is the minimum energy required for internal photoemission, denoted as the activation energy (Δ). A schematic of the equilibrium valence band alignment of the p-GaAs/Al_xGa_{1-x}As heterojunction is depicted in Fig. 1(b). The Al_xGa_{1-x}As barriers are intentionally graded to create an asymmetry, by tuning x, from $x_1 = 0.03$ at the bottom to $x_2 = 0.50$ at the top of each barrier. As a result, a potential gradient is built-up across the barrier. The valence band offsets at the p-GaAs/Al_xGa_{1-x}As interface,
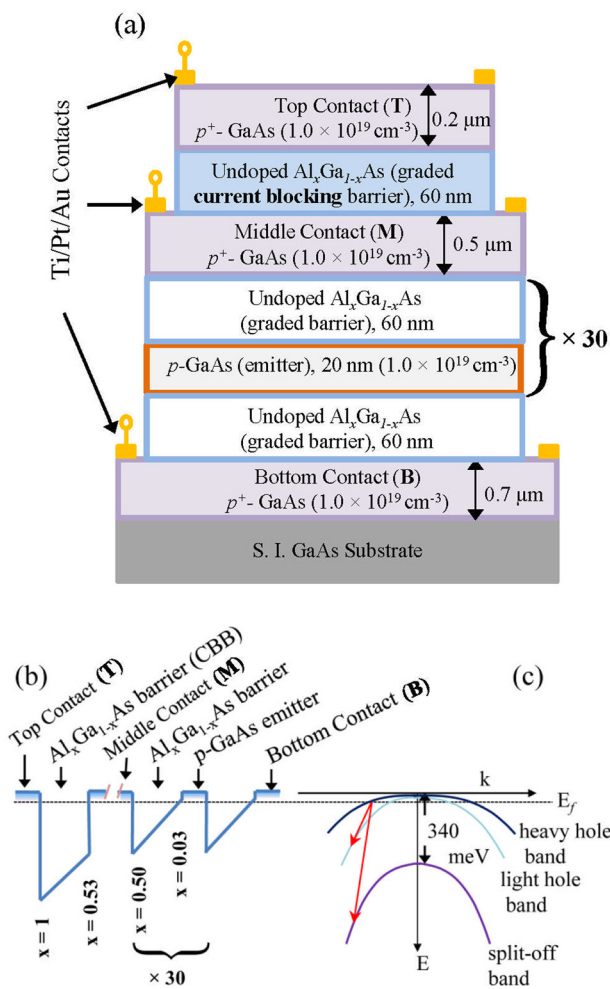
FIG. 1. (a) Schematic of the p-GaAs/Al$_x$Ga$_{1-x}$As heterostructure, including the current blocking barrier (CBB). The top (T) and bottom (B) contacts are used to measure with the CBB, and the middle (M) and bottom (B) contacts can be used to measure the same mesa without it. (b) Schematic of the valence band alignment under equilibrium. The Al$_x$Ga$_{1-x}$As barriers are graded by tuning the Al mole fraction, x. (c) A schematic of the valence band of the GaAs, showing some of the possible hole transitions from light hole/heavy hole to spin-orbit split-off bands, and also from the heavy hole to light hole band. The emitters are thick enough for bulk-like distribution of the density of states of carriers.
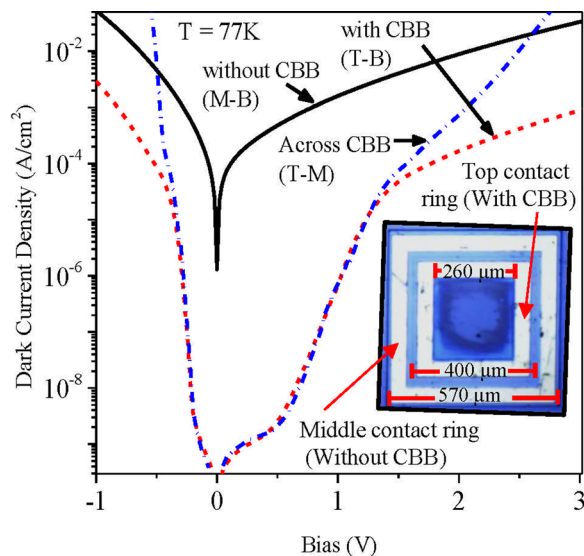

FIG. 2. The dark current density of the detector with CBB (T-B) is five orders of magnitude smaller at low bias, than without the CBB (M-B). The difference becomes smaller as the bias increases. The dark current across the top and middle (T-M) contacts is similar to that across T-B contacts in the low bias region. Inset: Top view optical image of the mesa showing the lateral dimensions of the top contact (400 μm × 400 μm) and middle contact (570 μm × 570 μm), with the optical window (260 μm × 260 μm) at the center.

calculated using the temperature-dependent internal photoemission (TDIPS) method,[20] are ∼17 meV and ∼280 meV for $x = 0.03$ and $x = 0.50$, respectively. This leads to an average potential gradient of ∼44 kV/cm across each Al$_x$Ga$_{1-x}$As barrier. Similarly, the Al$_x$Ga$_{1-x}$As CBB was graded by tuning x, from $x_1 = 0.53$ at the bottom to $x_2 = 1$ at the top, with valence band offsets of ∼290 meV and ∼550 meV, respectively, so that the potential gradient across it is also ∼44 kV/cm.

The Fermi level in the degenerately p-doped GaAs lies in the light hole (*LH*)/heavy hole (*HH*) band, with the spin-orbit split-off (*SO*) band separated by ∼340 meV from the *LH/HH* band near $k = 0$ (Fig. 1(c)). For IR detection, light absorption leads to hole transitions from the *LH/HH* bands to the *SO* band and from the *HH* to *LH* bands, and is followed by internal photoemission and escape of the holes over the barriers, which are swept out and collected at the contacts. A detailed account of possible escape pathways is provided elsewhere,[21] but the asymmetry of the Al$_x$Ga$_{1-x}$As barriers

plays an important role in driving the holes, even in the absence of an applied bias.

The current-voltage characteristics were measured at 77 K using a Keithley 2400 source meter and a Keithley 616 digital electrometer. Positive bias across T-B contacts is defined as the voltage connected to the top contact, with the bottom contact grounded. Similarly, in the M-B contacts measurements, voltage is connected to middle contact and the bottom contact is grounded, leaving the top contact open. In the measurements across top and middle (T-M) contacts, the voltage is connected to the top contact and middle contact is grounded, leaving the bottom contact open. The current voltage characteristics at 77 K are shown in Fig. 2, with the asymmetrical bias dependence of the dark current densities being a result of the asymmetrical barrier structure. We found that the CBB lowers the dark current density by as much as five orders of magnitude at low biases, with the difference becoming smaller as the bias increases. The differential resistance-area product (R_0A) at zero bias (not shown) with the CBB had a value of ∼7.2 × 10^8 Ω cm^2, compared to a value of 1.6 × 10^3 Ω cm^2 obtained without the CBB. The dark current measured across top and middle contacts (T-M) is similar to that measured across T-B contacts in the bias region <1.5 V. At low biases, the dc voltage is dropped across the different elements of the device in proportion to their dc resistances.[22] Therefore, most of the applied voltage will be dropped across the CBB, which has a high resistance compared to the rest of the device. The dark current is dominated by thermionic emission mechanism in the low voltage range, and by thermionic field emission (or thermal-assisted tunneling) in the high voltage range.[23] As the positive bias increases, the CBB assumes a sharper triangular shape and carrier transport by thermal-assisted tunneling (at least through the triangular part of the barrier) also increases, dominating the dark current beyond ∼0.5 V (>80 keV/cm).

For biases >1.5 V, however, the dark current measured across the T-B contacts deviates from that across the T-M contacts, indicating redistribution of the applied voltage across the whole structure (i.e., across T-B). As a result, carrier transport due to tunneling through the CBB and hence the dark current do not increase monotonically across T-B contacts, in contrast to that across T-M contacts.

The spectral responses were measured using a Perkin-Elmer system 2000 Fourier transform infrared (FTIR) spectrometer and calibrated using a Si composite bolometer of known sensitivity. The spectral responsivity at zero bias was measured in the same mesa both with and without the CBB. Specific detectivity (D*) under dark condition was obtained using

$$D^* = R_i \sqrt{\frac{R_0 A}{4kT}}, \qquad (1)$$

where R_i (A/W) is the spectral responsivity, k is the Boltzmann constant, T is the temperature, and A (cm^2) is the electrically active area of the detector (400 μm × 400 μm with the CBB, and 570 μm × 570 μm without the CBB). D* was found to be ∼1.9 × 10^{11} Jones at 2.7 μm for the detector with the CBB, and ∼4.1 × 10^8 Jones without the CBB. A two orders of magnitude higher D* is therefore obtained with the CBB at zero bias (Fig. 3(a)). As seen in Fig. 3(b), the 340 meV separation of the *SO* band from the *LH/HH* band limits the photoresponse from hole transitions between

the *LH/HH* and *SO* bands to ∼3.6 μm. Beyond 3.6 μm, there is a photoresponse due to the hole transitions between the *HH* and *LH* band. Therefore, two distinct response peaks are observed (without the CBB) at 2.7 μm and 5.0 μm, with responsivities of 0.67 mA/W and 0.38 mA/W, respectively. The 50% cut-off levels from these peaks encompass a ∼2–6 μm spectral range. With inclusion of the CBB, the measured responsivity of 0.47 mA/W at 2.7 μm is reduced by only a factor of ∼1.5 from that obtained without the CBB.

In order to understand the carrier injection mechanism under photovoltaic operation, we carried out photoresponse measurements in selective spectral ranges, using long-pass optical filters with characteristic cut-on wavelengths (λ_{CO}) to block the portion of the incident IR light with wavelengths shorter than the λ_{CO}. The photoresponse (corrected for the transmission of the filters) with the CBB was unaltered in the spectral range longer than λ_{CO}, with or without the optical filters ($\lambda_{CO} = 2.4$ μm and 4.5 μm), as seen in Fig. 3(b). Similar results were observed in measurements without the CBB (not shown). A photoresponse up to ∼2.4 μm was also observed across the T-M contacts (Fig. 3(c)) without a filter, closely agreeing with $\Delta = 550$ meV for the CBB. This photoresponse vanished, however, when an optical filter with $\lambda_{CO} = 2.4$ μm was implemented.

Since disabling the injection of photoexcited holes from the top contact to the middle contact (using the optical filter) did not affect the photoresponse of the detector with the
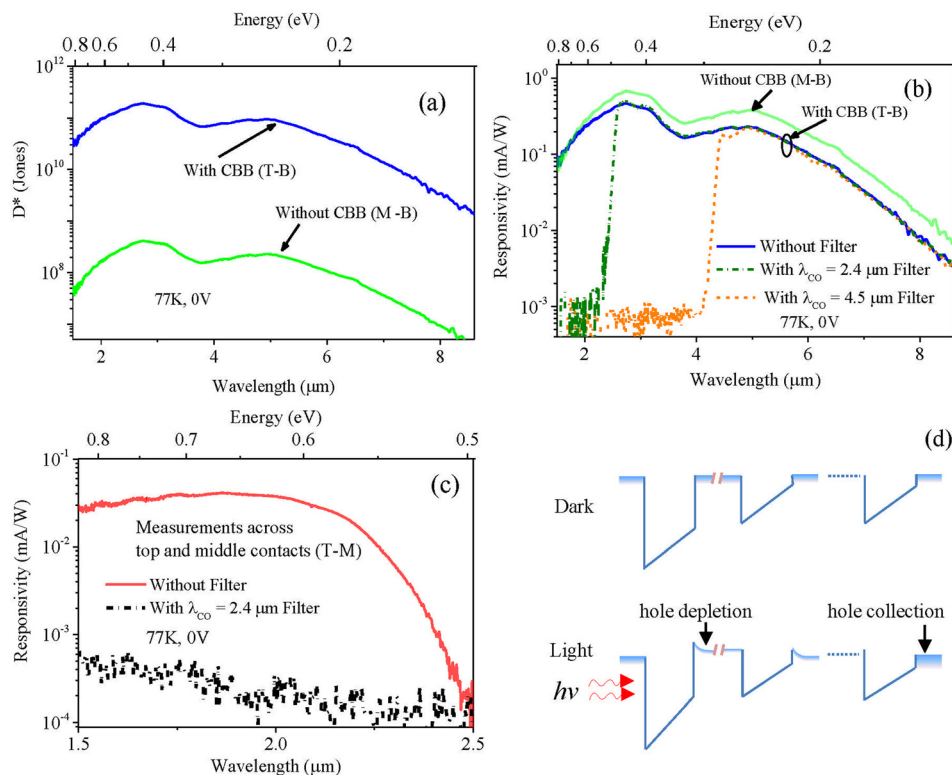

FIG. 3. (a) Comparison of the specific detectivity (D*) under dark conditions, showing a two orders of magnitude higher detectivity with the CBB. (b) Comparison of the spectral responsivity of the detector with the CBB, and without it. The two peaks at 2.7 μm and 5 μm are due to hole transitions from light/ heavy hole to split-off bands, and from heavy hole to light hole bands, respectively. The responsivity of the detector with the CBB is ∼1.5 times smaller at zero bias, than without the CBB. Introducing long-pass optical filters of cut-on wavelengths of $\lambda_{CO} = 2.4$ μm and 4.5 μm, with the CBB, did not show any effect on the photoresponse (corrected for the filters' transmission) in the spectral range longer than λ_{CO}. (c) The photoresponse below 2.4 μm, measured across the top and middle contacts, was disabled by the optical filter with $\lambda_{CO} = 2.4$ μm. (d) Schematic of valence bandstructure (without external field) in dark and under IR illumination showing hole depletion in the middle contact and eventual collection at the bottom contact. Owing to the hole depletion in the middle contact, an internal electric field builds up across the CBB.

CBB in the longer than λ_{CO} range, this means that there must be an alternative hole injection mechanism. In Ref. 6, carrier injection from a quantum well reservoir to an active region comprising quantum dots was achieved by carrier tunneling through a blocking barrier. However, the bulk-like distribution of energy states and rather thick CBB in our device rule out the possibility of hole injection through tunneling. In the absence of a large external electric field, thermal-assisted or photon-assisted tunneling processes are also unlikely to contribute to hole injection through the CBB to the middle contact. Instead, thermionic emission of holes over the CBB is most likely to refill the middle contact. Under IR illumination, the middle contact is depleted of holes owing to a net flow of the photoexcited holes towards the bottom contact, leading to eventual collection at the bottom contact (Fig. 3(d)). As a result, an electric field builds up across the CBB, acting like an internal field.[24] Then, net carrier transport towards the middle contact through a thermionic process is possible, thereby refilling the middle contact. The dependence of the thermionic emission mechanism on the barrier height and carrier mean free path requires further study to maximize detector performance.

The 0.5 μm thick p-GaAs middle contact layer serves as an extra terminal for comparison. However, it also absorbs a significant amount of light. In addition, carrier scattering in this thick layer may affect the performance, especially at higher temperatures. Therefore, in an optimized detector, this additional contact layer would be removed. Furthermore, the photoresponse of the detector can be improved in the 3–5 μm wavelength range, by further engineering the $Al_xGa_{1-x}As$ graded barriers, for example, by using undoped GaAs/$Al_xGa_{1-x}As$ superlattices,[25–27] rather than bulk $Al_xGa_{1-x}As$ layers.

In conclusion, we have demonstrated a 30 period p-GaAs/$Al_xGa_{1-x}As$ heterojunction IR photodetector in 2–6 μm range that incorporates a current blocking layer to give a two orders of magnitude increase in detectivity. Graded $Al_xGa_{1-x}As$ barriers enabled photovoltaic operation, leading to thermal noise limited performance at zero bias. The resistance-area product (R_0A) at zero bias was enhanced by five orders of magnitude due to the current blocking barrier, whilst the responsivity was reduced by only a factor of 1.5. The use of a current blocking barrier, together with graded barriers, opens up broad design avenues for the development of future p-GaAs/$Al_xGa_{1-x}As$ heterojunction detectors.

[1]S. Y. Wang, S. D. Lin, H. W. Wu, and C. P. Lee, Appl. Phys. Lett. **78**(8), 1023 (2001).

[2]P. Rotella, S. Raghavan, A. Stintz, B. Fuchs, S. Krishna, C. Morath, D. Le, and S. W. Kennerly, J. Cryst. Growth **251**(1–4), 787 (2003).

[3]S. Y. Wang, S. D. Lin, H. W. Wu, and C. P. Lee, Infrared Phys. Technol. **42**(3–5), 473 (2001).

[4]S. C. Lin, Y. R. Tsai, and S. C. Lee, Appl. Phys. Lett. **78**(18), 2784 (2001).

[5]D. Pal and E. Towe, in Proceedings of the 5th IEEE Conference on Nanotechnology (2005), Vol. 1, pp. 418–421.

[6]L. Nevou, V. Liverini, F. Castellano, A. Bismuto, and J. Faist, Appl. Phys. Lett. **97**(2), 023505 (2010).

[7]A. D. Stiff, S. Krishna, P. Bhattacharya, and S. W. Kennerly, IEEE J. Quantum Electron. **37**(11), 1412 (2001).

[8]S. F. Tang, S. Y. Lin, and S. C. Lee, Appl. Phys. Lett. **78**(17), 2428 (2001).

[9]S. Chakrabarti, A. D. Stiff-Roberts, P. Bhattacharya, S. Gunapala, S. Bandara, S. B. Rafol, and S. W. Kennerly, IEEE Photonics Technol. Lett. **16**(5), 1361 (2004).

[10]B. M. Nguyen, S. Bogdanov, S. A. Pour, and M. Razeghi, Appl. Phys. Lett. **95**(18), 183502 (2009).

[11]D. Z. Y. Ting, C. J. Hill, A. Soibel, S. A. Keo, J. M. Mumolo, J. Nguyen, and S. D. Gunapala, Appl. Phys. Lett. **95**(2), 023508 (2009).

[12]N. Gautam, H. S. Kim, M. N. Kutty, E. Plis, L. R. Dawson, and S. Krishna, Appl. Phys. Lett. **96**(23), 231107 (2010).

[13]S. Maimon and G. W. Wicks, Appl. Phys. Lett. **89**(15), 151109 (2006).

[14]H. S. Kim, O. O. Cellek, Z. Y. Lin, Z. Y. He, X. H. Zhao, S. Liu, H. Li, and Y. H. Zhang, Appl. Phys. Lett. **101**(16), 161114 (2012).

[15]P. Klipstein, Proc. SPIE **6940**, 69402U (2008).

[16]A. G. U. Perera, S. G. Matsik, B. Yaldiz, H. C. Liu, A. Shen, M. Gao, Z. R. Wasilewski, and M. Buchanan, Appl. Phys. Lett. **78**(15), 2241 (2001).

[17]P. V. V. Jayaweera, S. G. Matsik, A. G. U. Perera, H. C. Liu, M. Buchanan, and Z. R. Wasilewski, Appl. Phys. Lett. **93**(2), 021105 (2008).

[18]P. K. D. D. P. Pitigala, S. G. Matsik, A. G. U. Perera, S. P. Khanna, L. H. Li, E. H. Linfield, Z. R. Wasilewski, M. Buchanan, and H. C. Liu, J. Appl. Phys. **111**(8), 084505 (2012).

[19]L. H. Li, J. X. Zhu, L. Chen, A. G. Davies, and E. H. Linfield, Opt. Express **23**(3), 2720 (2015).

[20]Y. F. Lao and A. G. U. Perera, Phys. Rev. B **86**(19), 195315 (2012).

[21]A. G. U. Perera, S. G. Matsik, P. V. V. Jayaweera, K. Tennakone, H. C. Liu, M. Buchanan, G. Von Winckel, A. Stintz, and S. Krishna, Appl. Phys. Lett. **89**(13), 131118 (2006).

[22]H. C. Liu, J. Li, J. R. Thompson, Z. R. Wasilewski, M. Buchanan, and J. G. Simmons, IEEE Trans. Electron Devices **40**(11), 2142 (1993).

[23]H. X. Yuan and A. G. U. Perera, Appl. Phys. Lett. **66**(17), 2262 (1995).

[24]H. Schneider, C. Schönbein, M. Walther, K. Schwarz, J. Fleissner, and P. Koidl, Appl. Phys. Lett. **71**(2), 246 (1997).

[25]K. K. Choi, M. D. Jhabvala, and R. J. Peralta, IEEE Electron Device Lett. **29**(9), 1011 (2008).

[26]L. S. Yu, S. S. Li, and P. Ho, Appl. Phys. Lett. **59**(21), 2712 (1991).

[27]L. S. Yu, Y. H. Wang, S. S. Li, and P. Ho, Appl. Phys. Lett. **60**(8), 992 (1992).